Journal of MATERIALS RESEARCH

Invited Paper
DOI:10.1557/s43578-021-00328-w

EARLY CAREER SCHOLARS IN MATERIALS SCIENCE 2022

ANNUAL ISSUE

Salt-rejecting rGO-coated melamine foams for high-efficiency solar desalination

Chao Chang[1,a], Min Liu[1], Lanxin Li[1], Guowei Chen[1], Lilin Pei[1], Zongyu Wang[1,a], Yulong Ji[1]

[1] *Institute of Marine Engineering and Thermal Science, Marine Engineering College, Dalian Maritime University, Dalian 116026, People's Republic of China*

[a] Address all correspondence to these authors. e-mails: chang3223426@126.com; wangzongyu09@163.com

Received: 6 June 2021; accepted: 3 August 2021; published online: 18 October 2021

Solar-driven interfacial desalination has been emerged as a promising water treatment technology to generate drinkable water out of seawater. The accumulated salt crystals generated from seawater, however, have adverse effects on solar-driven interfacial evaporation. In this work, we prepared a salt-rejecting reduced graphene oxide (rGO) foam by depositing rGO particles on a hydrophilic melamine foam for solar desalination. Benefitting from the intrinsic porous microstructure and hydrophilicity, the rGO-coated melamine foam has sufficient wettability to draw water to the evaporation region, leading to rapid replenishment of water and simultaneously avoiding salt precipitation. Based on the rGO-coated melamine foam, the interfacial evaporation system can achieve a steady-state evaporation efficiency of 89.6% under a solar flux of 1 kW m^{-2} and has good durability under one sun over 12 h. With the high solar-to-thermal conversion efficiency and excellent long-term stability, this interfacial evaporation system exhibits the potential of commercial seawater desalination.

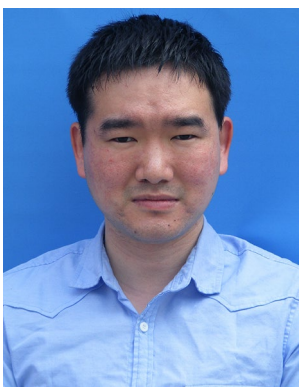

Chao Chang

is a lecturer of the Marine Engineering College at the Dalian Maritime University. He received his bachelor degree and master degree in Marine Engineering from the Dalian Maritime University in 2012 and 2015, respectively. He completed his PhD degree in the School of Materials Science and Engineering at the Shanghai Jiao Tong University in 2019. Since July 2019, he has been a faculty member as a lecturer in the Marine Engineering College at the Dalian Maritime University. Chang's interest is in the area of the nanomaterials, phase change heat transfer, heat pipe technology and thermal management technology. He is particularly focused on the synthesis and preparation of solar thermal conversion materials, the heat transfer mechanism of solar thermal energy conversion and the design solar thermal harvesting devices. His primary focus is on the fluid flow and heat transfer mechanism of oscillating heat pipes and the optimization of the oscillating heat pipe's structure, enabling the development of advanced heat pipes for thermal management of high power devices or waste heat recovery. Much of the group's work has been in solar thermal conversion technology including solar steam generation, solar seawater desalination, solar heat pipe technology and phase change materials for solar thermal energy storage.

Introduction

Nowadays, the global energy crisis and water shortage have become major threats to the sustainable development of human society [1, 2]. To meet the growing demand of energy, the developments of various high-performance energy conversion and water purification technologies have attracted increasingly attentions [3]. Solar energy as one of the promising renewable energy sources has shown potential to replace the finite reserved fossil fuels due to its extremely large capacity, ubiquity, cleanness and capability of versatile conversion [4]. Besides the direct electric energy generation by photovoltaic technology, the solar-to-thermal energy conversion technology, which absorbs solar energy and converts it into thermal energy, it is considered as a facile and efficient way to harness solar energy [5]. The converted thermal energy can drive important industrial processes such as solar-thermal power station, solar desalination, sterilization, solar heating water system and other heat-related applications. Solar desalination provides an attractive solution to extract fresh water from seawater through solar-to-thermal conversion processes without extra energy input, especially for the developing countries and islands which lack of basic infrastructures [6–8]. In recent years, the solar-driven interfacial evaporation technology, which localizes solar-to-thermal conversion process at the liquid–vapor interface, has emerged as a new type of solar utilization technology [9–12]. Compared to conventional bulk heating, the interfacial evaporation system has demonstrated higher evaporation efficiency and faster thermal response, and it offers a potential alternative in seawater desalination.

Since the first interfacial evaporation technology was proposed by Chen et al. [13], there have been many investigations to improve the thermal performance of interfacial evaporation systems. A typical solar-driven interfacial evaporation system consists of three important components: a solar absorber which has high solar absorption and efficiently converts solar irradiation into thermal energy; a thermal insulator which suppresses the converted heat energy transferred to the bulk water; and a water supply path which continuously and efficiently wicks water from the bulk water to the surface of solar absorber. In previous research, tremendous efforts have been devoted to enhancing the overall solar-to-vapor conversion efficiency by synthesizing broadband and efficient solar absorbing materials [14–17], optimizing the structure of solar absorbers [18–20] designing new water supplying path [21, 22] and improving thermal insulation structure [23, 24]. So far, the solar-driven interfacial evaporation system has been served for many industrial processes, inducing solar distillation [25], solar sterilization [26], solar desalination [27–29] and solar power generation [30, 31]. To achieve high evaporation performance of the system, the first strategy is to explore solar absorbing materials for broadband absorption across the solar spectrum. Currently, the solar absorbing materials developed and explored for the solar-driven interfacial evaporation system mainly contain carbonaceous materials, plasmonic particles and spectra selective absorbing materials [32–34]. Among them, the naturally black, carbonaceous materials demonstrate strong solar-to-thermal conversion capability and are suitable for broadband and high-efficiency solar absorbers. Due to the high solar absorptance, low cost and good stability, many carbon-based solar absorbers have been investigated including carbon nanotube [35, 36], graphite [37] and reduced graphene oxide [38]. After many years of efforts, the solar-to-vapor conversion efficiency of the system has achieved more than 90% under 1 sun illumination.

Although great improvements have been made in developing the solar absorbing materials and designing the interfacial evaporation structures, most of previously reported solar desalination devices suffer from the salt accumulation on the top surface of the evaporator during desalination. The accumulated salts hinder solar absorption and block the porous evaporator, resulting in low solar-to-thermal conversion efficiency and poor evaporation performance. Conventional physical methods such as sonication and water immersion are generally used to remove the accumulated salts, but these methods are easy to cause the damage of the interfacial evaporation structure. To mitigate the accumulation of salts in the interfacial evaporation system, many researches focus on developing hydrophobic evaporators [39, 40]. The hydrophobic evaporators, however, limit the water supply to the top surface, which deteriorate the evaporation performance of the system. Another method to address this problem is to use hydrophilic evaporators, which enables the excess salts to move from the top surface to the bulk water [41, 42]. To date, many investigations focused on designing hydrophilic evaporators, such as hydrophilic cellulose fabric membranes, paper-based hydrophilic membranes and bioinspired evaporators. However, development of a long-term stable and highly efficient solar-driven interfacial evaporation system is still a major challenge.

In this work, we demonstrate a salt-rejecting, highly efficient solar absorption and fast thermal response reduced graphene oxide (rGO) foam for solar-driven interfacial desalination under low-flux solar illumination. In the new porous construction, a hydrophilic melamine foam (MF) was selected as substrate, which not only enlarged the surface area for solar absorption, but also enhanced multiple scatter. The surface hydrophilicity and porosity of the rGO-coated melamine foam provided sufficient wetting and fluid flow of the bulk saline water to the solar-to-thermal conversion region, leading to rapid replenishment of water and simultaneously avoiding salt accumulation. Taking advantage of the high performance of the rGO-coated melamine foam, the solar-driven interfacial system was able to achieve a solar-to-vapor conversion efficiency of 89.6% under 1

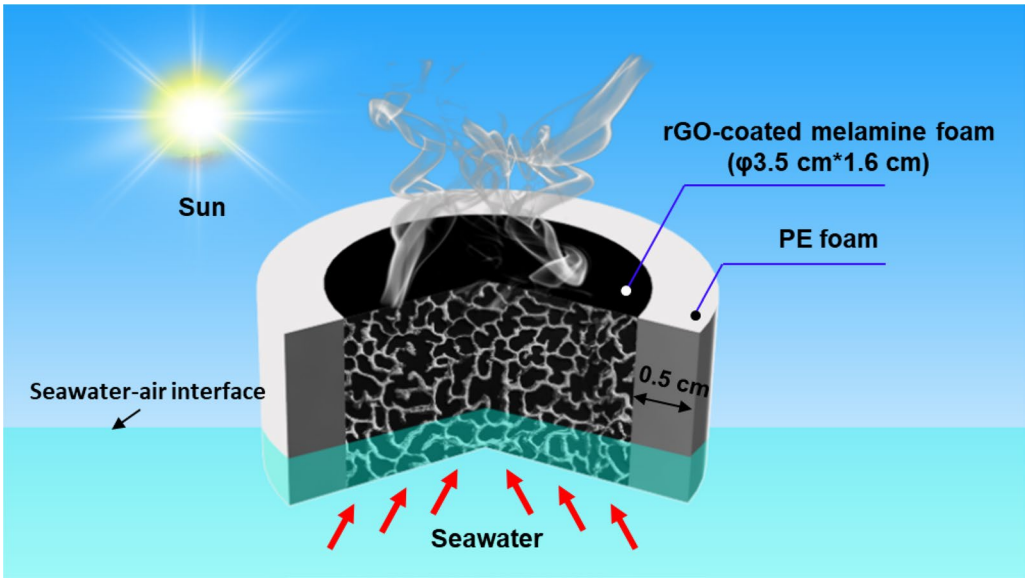

Figure 1: Schematic illustration of the interfacial evaporation system based on the rGO-coated melamine foam for solar desalination.

sun illumination. In addition, a solar-driven interfacial desalination device was designed and fabricated by integrating the rGO-coated melamine foam into a commercial solar still, which had a solar-to-water conversion efficiency of 56.4% under 1 sun illumination. After solar desalination, the collected clean water was of drinkable quality requirements. Due to the superior evaporation performance and scalability of solar-to-thermal conversion materials, our solar-driven interfacial desalination

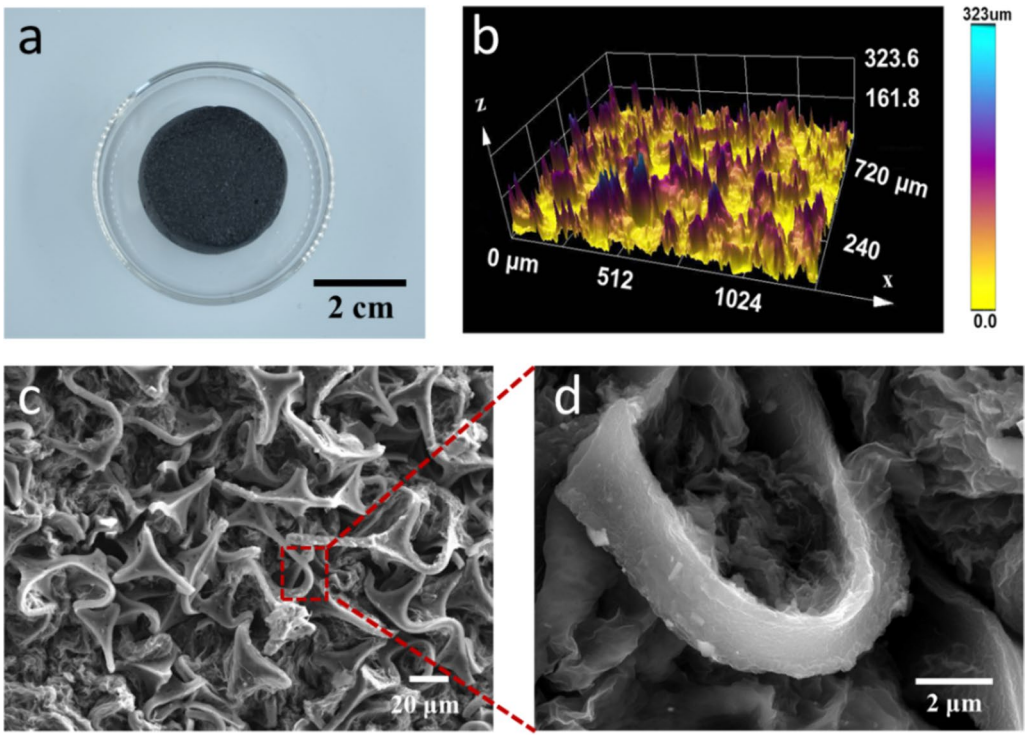

Figure 2: (a) A photograph of the fabricated rGO-coated melamine foam with a dimeter of 3.5 cm. (b) 3D optical microscopic image of the rGO-coated melamine foam. (c) SEM image of the rGO-coated melamine foam under low magnification. (d) SEM image of the rGO-coated melamine foam under high magnification.

system presents a broad prospect in the practical application of seawater desalination.

Results and discussion

The schematic of the interfacial evaporation system based on the rGO-coated melamine foam for solar desalination is shown in Fig. 1. The rGO-coated melamine foam is localized in the middle and its outside is wrapped by a layer of polyethylene (PE) foam to construct a self-floating interfacial evaporation system. The rGO-coated melamine foam was used to effectively absorb incident solar radiation and convert solar energy into heat to generate the driving force for interfacial evaporation. On the other hand, the hydrophilic rGO-coated melamine foam could continually wick salt water to the evaporation region. The porous structure of the rGO-coated melamine foam allowed the generated vapor to escape into the environment and facilitated solar light capturing, thereby improving solar-to-thermal conversion efficiency. The rGO-coated melamine foam was porous and hydrophilic, allowing it to wick water to the evaporative structure above, while diffusing concentrated salt down back into the bulk seawater. During the evaporation process, the salt concentration at the foam increased above the concentration of seawater at the bottom. The concentration difference would drive the salt to diffuse into the bulk water. Additionally, the surrounding PE foam not only enabled the rGO-coated melamine foam to naturally float on the water surface, but also suppressed heat loss by the surrounding salt water. Without complicated construction design, our interfacial evaporation system could continuously and efficiently operate on the water surface. In addition, as the evaporation occurred at the vapor–liquid interface, the interfacial evaporation system could autonomously move when the interface receded.

The rGO-coated melamine foam is the key component of the interfacial evaporation system. We prepared the rGO-coated melamine foam by immersing the melamine foam into the GO colloidal suspension, and then reduced the GO into rGO by a hydrothermal method. Figure 2a presents that the rGO-coated melamine foam with a diameter of 3.5 cm and a thickness of 1.6 cm can be easily fabricated, and it has a dark black color. Figure 2b shows the roughness of the surface of the rGO-coated melamine foam which is observed using a 3D optical microscopy. The resulting image indicates that the height change reaches more than 300 μm. The rough surface structure of the solar-thermal conversion composites is mainly attributed to the porous structure of melamine foam and the modified rGO also increases the roughness of the surface. The surface roughness amplifies the solar absorbing surface area, and simultaneously increase multi-scattering of incident solar light, thereby improving the solar-to-thermal conversion efficiency of the system. Figure 2c, d show the microstructure of the prepared rGO-coated melamine foam under different magnifications. As shown, the surface of rGO-coated melamine foam presents a wrinkled and interconnected network structure, and the pore size of the rGO-coated melamine foam is ranging from 20 to 40 μm. The open pore structure and wrinkled surface facilitate to GO deposition.

Due to the hydrophilicity of the porous melamine foam, the rGO-coated melamine foam presents excellent water wettability. Once a water droplet contacted the surface of the rGO-coated melamine foam, it was completely absorbed within 0.5 s. The hydrophilic surface of rGO composites could effectively channel the water flow within the porous structure. The porosity of the rGO-coated melamine foam was also measured by comparing the mass changes before and after absorbing water. The porosity of prepared rGO-coated melamine foam could reach up to 85.55%. Solar absorption of the rGO-coated melamine foam directly affected the solar-to-thermal conversion efficiency of the system.

The absorption spectrum of the rGO-coated melamine foam was detected via an ultraviolet–visible–near-infrared

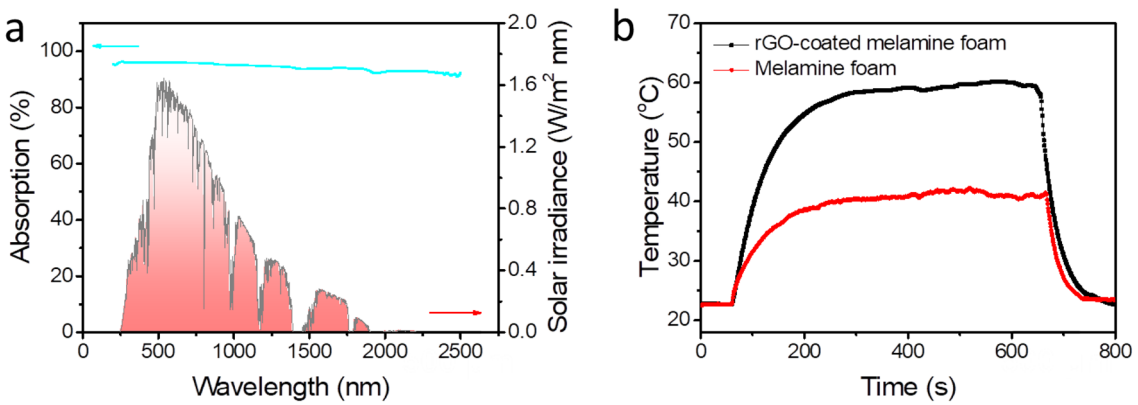

Figure 3: (a) Ultraviolet–visible–near-infrared (UV–Vis–NIR) absorption spectra of the rGO-coated melamine foam. (b) Temperature evolution of the dry rGO-coated and untreated melamine foams under the solar power density of 1 kW m^{-2}.

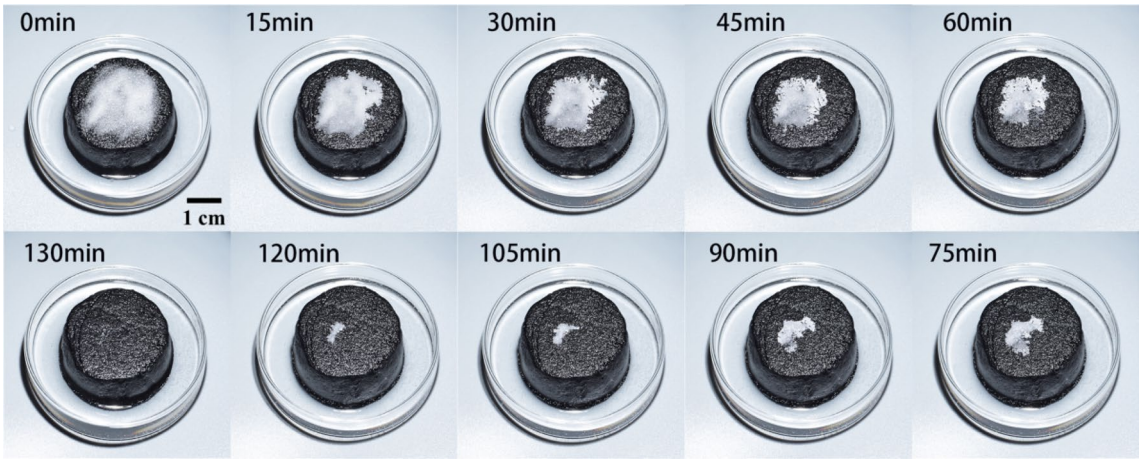

Figure 4: Salt-rejecting performance of the rGO-coated melamine foam evaporator.

(UV–Vis–NIR) spectrophotometer with an integrating sphere as shown in Fig. 3a. The rGO-coated melamine foam has a high broadband absorption of 94.4% ranging from 250 to 2500 nm, which completely covers the solar irradiance spectrum, meaning that it can efficiently convert incident solar energy into heat for driving interfacial evaporation. To further demonstrate the solar-to-thermal conversion property, the dry rGO-coated melamine foam and pristine melamine foam were placed under the same solar power density of 1 kW m^{-2}. As shown in Fig. 3b, the surface temperature of the rGO foam quickly rises to 60 °C, while the untreated melamine foam temperature is only heated to 40 °C under the same solar illumination. Clearly, the porous rGO-coated melamine foam has a faster thermal response and better solar-to-thermal conversion capability than the uncoated melamine foam.

To evaluate the salt-rejecting capability, the rGO-coated melamine foam was placed in the NaCl solution (3.5 wt%), and 3 g solid NaCl was placed on the top surface as shown in Fig. 4. The rGO-coated melamine foam was then placed under the solar power density of 1 kW m^{-2}. The amount of solid salt is gradually dissolved after 120 min. The pores in the rGO-coated melamine foam allow for pumping water flow to the top surface of the evaporator. When the sunlight was shining on the top surface of the rGO-coated melamine foam, the temperature of the rGO-coated melamine foam rapidly increased within minutes, and remained constant at 35 °C during the entire evaporation process. Because the solubility of salt depends on temperature, the higher temperature accelerates the dissolution of the salt, so that the salt irons could be re-dissolved into the water on the surface. The innumerable pores in the rGO-coated melamine foam with high water absorption capacity could provide continuous water supply to the top surface, and salt could move from the top surface to the sublayer of water. The difference in temperature led to the difference in salinity between the upper evaporation surface and the bulk water, and the salinity difference was the driving force for salt movement from upper evaporation layer to the bulk water. Therefore, the hydrophilicity and porosity of the rGO-coated melamine foam could achieve a high water sorption rate, which ensure that the accumulated salts on the top surface of the evaporator are dissolved and moved to the bulk water.

To evaluate the solar-to-vapor conversion performance of the interfacial evaporation system, a Xenon lamp was used as the solar simulator from 0.3 sun (0.3 kW m^{-2}) to 1 sun (1 kW m^{-2}). The surface temperature of the evaporator was monitored by a

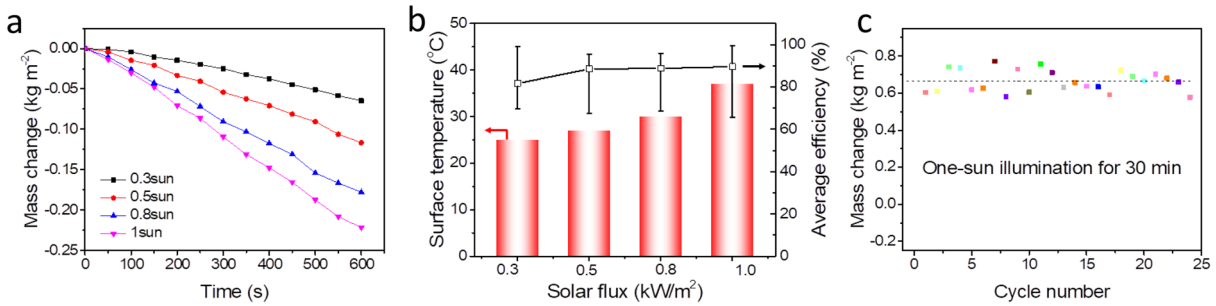

Figure 5: (a) Steady-state water evaporation flux of the interfacial evaporation system. (b) Comparison of surface temperature and average solar-to-vapor conversion efficiency under different solar fluxes. (c) Evaporation cycle performance of the interfacial evaporation system under 1 sun illumination.

TABLE 1: Performance comparison between rGO-coated melamine foams evaporator and other interfacial evaporation materials under 1 sun illumination.

Researchers	Materials	Evaporation efficiency (%)	Evaporation rate(kg m^{-2} h^{-1})
Zhou et al. [12]	Gold nanoparticles absorber	64	0.9
Zhou et al. [14]	Aluminum nanoparticles absorber	57	1.0
Bae et al. [15]	Flexible thin-film black gold membranes	48	0.5
Chang et al. [17]	TiNO absorber	80.5	1.33
Zhu et al. [25]	Cellular carbon sponge	85	1.31
Kuang et al. [27]	Natural wood solar evaporator	75	1.04
Yang et al. [30]	Carbon nanotube modified filter paper	73	1.1
Zhu et al. [31]	3D organic bucky sponge	87.4	1.33
Yin et al. [36]	Vertically aligned carbon nanotube array	30	1.0
Zhao et al. [40]	Ti_3C_2 nanosheet layer	71	1.31
This work	rGO-coated melamine foams	89.6	1.43

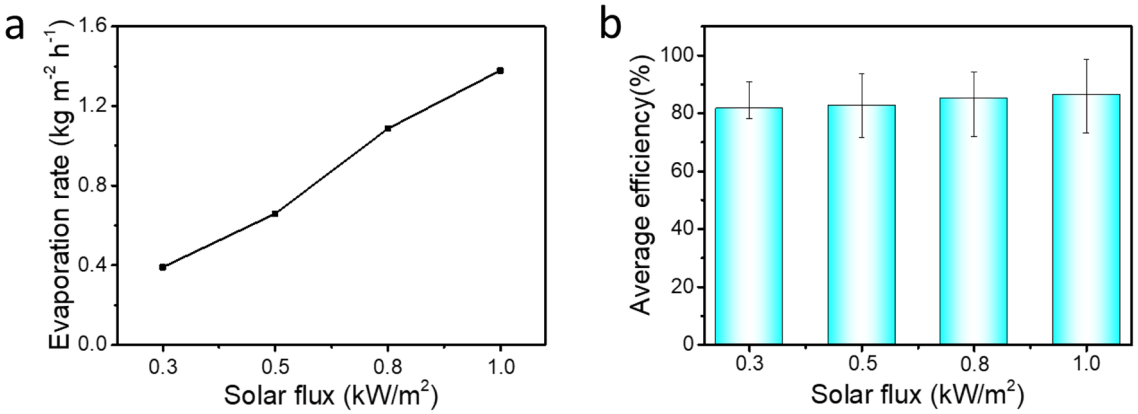

Figure 6: (a) Steady-state seawater evaporation rate of the interfacial evaporation system. (b) Comparison of average seawater evaporation efficiency under different solar fluxes.

thermocouple. The thermocouple was placed in the center of the top surface of the evaporator. The interfacial evaporation efficiency (η_{water}) is determined by the following equation:

$$\eta_{water} = \frac{m_{water} h}{q_{solar} A} \quad (1)$$

where m_{water} is the evaporation mass flux, h is the total latent heat of water during the interfacial evaporation process which includes both latent heat and sensible heat, q_{solar} is the incident solar flux and A is the cross-sectional surface area of the rGO-coated melamine foam.

Figure 5a shows the water mass changes of the solar-driven interfacial evaporation system at different solar fluxes. The evaporation mass changes of the system increase at the larger solar power densities. In the evaporation process, the evaporated water mass change of the interfacial evaporation system is 0.064 kg m^{-2} under the solar power density of 0.3 kW m^{-2}. When the solar flux is 1 kW m^{-2}, the evaporated mass change increases to 0.221 kg m^{-2}. The water evaporation rate of the interfacial evaporation system increases from 0.42 to 1.43 kg m^{-2} h^{-1} with the solar flux increasing from 0.3 to 1 kW m^{-2}. According to Eq. (1), the corresponding solar-to-vapor conversion efficiencies at different solar fluxes are obtained. As shown in Fig. 5b, the solar-to-vapor conversion efficiency of the rGO-based interfacial evaporation system can reach up to more than 80% under the solar power density of 0.5 kW m^{-2}, and the efficiency is up to 89.6% when the solar flux is 1 kW m^{-2}. We also compared our interfacial evaporation system based on rGO-coated melamine foams to other interfacial evaporation systems as shown in Table 1. The results show that our interfacial evaporation system can realize high evaporation performance under 1 sun illumination.

The durability is a key factor on the thermal performance of the interfacial evaporation system. Figure 5c shows the cycle evaporation performance of the interfacial evaporation system under the solar power density of 1 kW m^{-2}. The mass changes

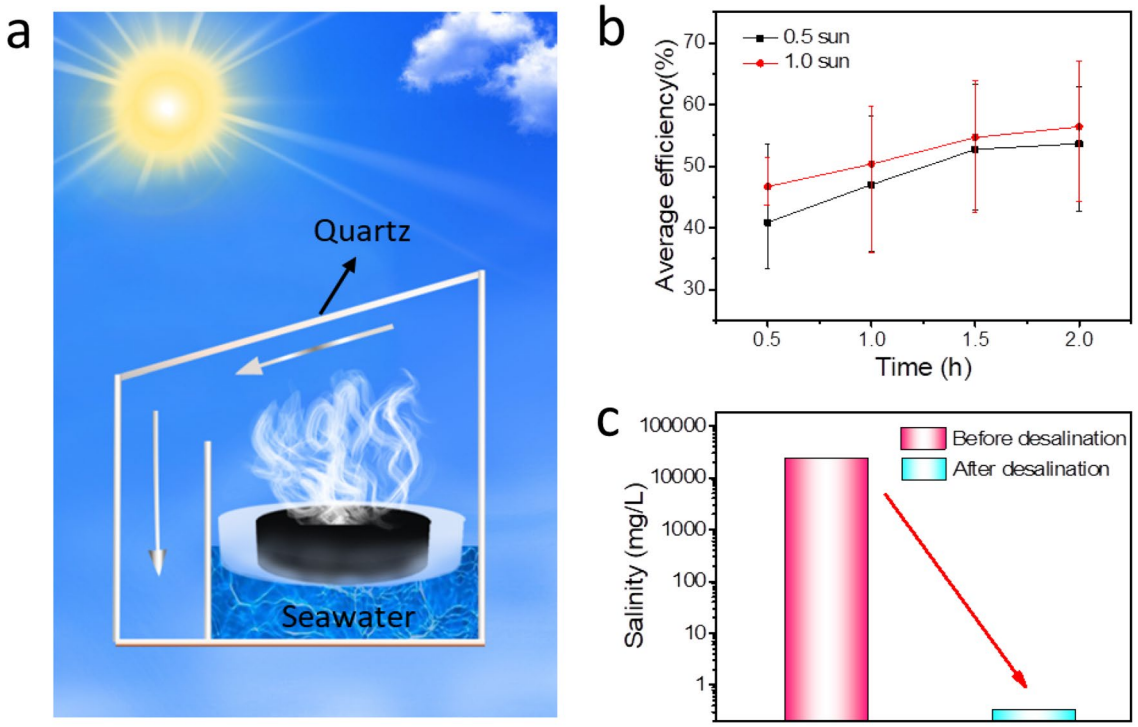

Figure 7: (a) Schematic illustration of the experimental setup of the solar still with the rGO-coated melamine foam for seawater desalination. (b) Average desalination efficiency of the solar still under 0.5 sun and 1 sun illumination. (c) Comparison of salinity between seawater and collected condensed water.

are kept at an average of 0.65 kg m^{-2} even after 25 times cycle, and each evaporation cycle is sustained for 0.5 h. This result indicates that the interfacial system has excellent stability and durability over long-term cycles.

Additionally, the seawater evaporation performance of the interfacial evaporation system was measured under different solar fluxes as shown in Fig. 6. The evaporation rate of seawater in the interfacial evaporation system increases from 0.39 to 1.41 kg m^{-2} h^{-1} with the solar flux increasing from 0.3 to 1 kW m^{-2}. In the same way, the corresponding evaporation efficiency of the interfacial evaporation system is increasing from 80 to 86%. Compared to water, the seawater evaporation efficiency of the interfacial evaporation system is almost unchanged. Besides high solar-to-thermal conversion efficiency, accumulated salt is not observed on the surface of the rGO-coated melamine foam. This is because that the excellent hydrophilicity and porosity of the rGO-coated melamine foam evaporator can absorb seawater from the bulk water and simultaneously quickly dissolve the salt accumulated on the top surface of the foam, thereby resulting in the salt-rejecting capability.

Finally, we demonstrated the rGO-coated melamine foam for the application of seawater desalination as shown in Fig. 7a. The rGO-coated melamine foam evaporator was placed on the surface of a NaCl aqueous solution (3.5 wt%), which was used to simulate the seawater. A transparent glass cover was localized at the top of the desalination device. The cover had a transmittance of 92% and allowed incident solar light incident onto the saline solution. To reduce heat loss, we wrapped the sidewalls and the bottom of the device by thermal insulation materials. Under solar illumination, the sunlight passed through the transparent glass cover and was incident into the device. The floating rGO-coated melamine foam evaporator absorbed solar energy and thermally vaporized the water at the vapor–liquid interface. The steady steam generated from the vapor–liquid interface diffuses to the surface of the cover, and condenses into water. The purified water flows into the clean water receptacle with the assistance of gravity. We calculated the solar-to-water conversion efficiency by the following equation:

$$\eta_{\text{water}} = \frac{m'_{\text{water}} h_{\text{fg}}}{q_{\text{solar}} A} \tag{2}$$

where m'_{water} is the mass flux of condensed clean water, h_{fg} is the phase change enthalpy of seawater, q_{solar} is the incident solar and A is the surface area of the rGO-coated melamine foam. Figure 7b presents the solar-driven interfacial desalination performance under different solar power densities. The solar-to-water conversion efficiency of our solar still was determined using Eq. (2) to be 53.6% under the solar power density of 0.5 kW m^{-2}, and the efficiency increases to 56.4% under the solar power density of 1 kW m^{-2}. Although the solar-to-vapor conversion efficiency of the rGO-based interfacial evaporator

was up to 90%, the maximum solar-to-water conversion efficiency was only 56.4%. The reason is that the absorbed solar energy is partially transported from the top glass plate to the atmosphere. No NaCl crystals were observed on the surface of the evaporator during the evaporation process. After evaporation, the excess Na^+ would move back to the underneath saline water with the assistance of salinity difference between the interfacial evaporator and bulk water.

We used an inductively coupled plasma spectroscopy (ICP-MS) to detect the concentration of ions in the collected clean water. Comparing the simulated seawater and the collected water in Fig. 7c, the concentration of Na^+ in the collected clean water drops from 23,600 to 0.326 mg/L after solar-driven desalination, meets the World Health Organization (WHO) standards [43] for drinkable water. Consequently, benefiting from the salt-rejecting process and the excellent solar-to-thermal conversion capability, our interfacial evaporation system shows the potential to lower the cost, improve the efficiency of seawater desalination and further broaden the scope of application.

Conclusion

In this work, we demonstrated a stable, salt-rejecting, highly efficient and fast thermal response rGO-coated melamine foam for solar-driven interfacial desalination under low-flux solar illumination. To obtain the broadband and efficient solar absorption, a porous hydrophilic melamine foam was modified by coating it with the rGO particle, resulting in increased solar energy absorption surface area and increasing multiple scatter. The solar interfacial evaporation system based on the rGO-coated melamine foam showed a quickly thermal response and achieved steady-state solar-to-thermal conversion efficiency of 89.6% under the solar power density of 1 kW m^{-2}. Finally, we integrated the rGO-coated melamine foam evaporator into a solar still, which could produce potable water with an efficiency of 56.4% under the solar power density of 1 kW m^{-2} and inhabit salt accumulation. We expected that such a solar-driven interfacial desalination device could be applied on the isolated islands or for survival at the sea to collect drinkable water from the abundant seawater or other saline water resources. These unique features of our new interfacial evaporation structure such as efficient desalination efficiency, salt-rejecting property offer a potential to alleviate the problem of clean water shortage in remote underdeveloped regions.

Experimental section

Materials

The melamine foam (density: 9 kg/m^3, porosity: 99%) was brought from Shanghai Bayou Building Materials Co., Ltd. Aqueous colloidal suspension of graphene oxide (GO, thickness: 0.6 ~ 1.0 nm, diameter: 0.5 ~ 5 um, concentration: 5 mg/mL) was ordered from Xiamen Knano Graphene Technology Co., Ltd. Sodium chloride, ethanol and acetone were brought from Shanghai Aladdin Chemical Reagent Co., Ltd. All the reagents used in the experiments were of analytical grade and used without further purification. Deionized (DI) water was used in all the experiments.

Preparation of the rGO-coated melamine foam

In the typical synthesis process of the rGO-coated melamine foam, the commercial melamine foam with a dimeter of 3.5 cm and a thickness of 1.6 cm was first rinsed with ethanol and DI water in turn for 30 min, and dried. The melamine foam was then soaked in GO aqueous suspension for 30 min to obtain a GO-coated melamine foam. To reduce GO foam into rGO, the sample was placed in a 100 ml Teflon autoclave which contained 20 ml of DI water and 10 ml of ethanol, and was hydrothermally treated at 120 °C for 3 h. Last, the sample was dried in an oven to obtain the rGO-coated melamine foam.

Measurement and characterization

The microstructure of the rGO-coated melamine foam was observed by a field emission scanning electron microscope (SEM, Sirion 2000, FEI). Absorption spectrum of the rGO-coated melamine foam was measured with an ultraviolet–visible–near-infrared (UV–Vis–NIR) spectrometer (PerkinElmer, Lambda 750S). The 3D optical microscope images of the sample were measured by a 3D digital microscope (Keyence VHX-S50). The salinity of the water before and after solar desalination was measured by Inductively Coupled Plasma Optical Emission Spectrometry (ICAP7600).

Simulated solar desalination experiment

A solar simulator (CEL-PE300L-3A, Beijing China Education Au-light Technology Co., Ltd.) was used to generate the large-flux solar illumination, and a solar power meter (CEL-NP2000-2A, Beijing China Education Au-light Technology) was used to check the illumination intensity. Mass change of the solar-driven interfacial evaporation system was recorded with a digital balance (BSM-120.4, Shanghai Zhuojing Electronic Technology Co., Ltd). All the experiments were carried out at a temperature of 20 ± 2 °C and a relative humidity of 55 ± 5%.

Acknowledgments

This work was financially supported by Joint Research Fund Liaoning-Shenyang National Laboratory for Materials Science (Grant No. 2019JH3/30100007), the Fundamental

Research Funds for the Central Universities of China (Grant No. 3132019331), China Postdoctoral Science Foundation (Grant No. 2020M670724) and the National Key Research and Development Program of China (Grant No. 2019YFE0116400).

Data availability

The data in the current study are available from the corresponding author on reasonable request.

Open Access

References

1. P.J.J. Alvarez, C.K. Chan, M. Elimelech, N.J. Halas, D. Villagrán, Emerging opportunities for nanotechnology to enhance water security. Nat. Nanotechnol. **13**(8), 634 (2018)
2. C.J. Vörösmarty, P. Green, J. Salisbury, R.B. Lammers, Global water resources: vulnerability from climate change and population growth. Science **289**(5477), 284 (2000)
3. M.A. Abdelkareem, M. El Haj Assad, E.T. Sayed, B. Soudan, Recent progress in the use of renewable energy sources to power water desalination plants. Desalination **435**, 97 (2018)
4. N.S. Lewis, Research opportunities to advance solar energy utilization. Science **351**(6271), aad1920 (2016)
5. M. Thirugnanasambandam, S. Iniyan, R. Goic, A review of solar thermal technologies. Renew. Sustain. Energy Rev. **14**(1), 312 (2010)
6. M. Elimelech, W.A. Phillip, The future of seawater desalination: energy, technology, and the environment. Science **333**(6043), 712 (2011)
7. M. Gao, L. Zhu, C.K. Peh, G.W. Ho, Solar absorber material and system designs for photothermal water vaporization towards clean water and energy production. Energy Environ. Sci. **12**(3), 841 (2019)
8. M.T. Ali, H.E.S. Fath, P.R. Armstrong, A comprehensive techno-economical review of indirect solar desalination. Renew. Sustain. Energy Rev. **15**(8), 4187 (2011)
9. P. Tao, G. Ni, C. Song, W. Shang, J. Wu, J. Zhu, G. Chen, T. Deng, Solar-driven interfacial evaporation. Nat Energy **3**(12), 1031 (2018)
10. L. Zhu, M. Gao, C.K.N. Peh, G.W. Ho, Recent progress in solar-driven interfacial water evaporation: advanced designs and applications. Nano Energy **57**, 507 (2019)
11. C. Chen, Y. Kuang, L. Hu, Challenges and opportunities for solar evaporation. Joule **3**(3), 683 (2019)
12. X. Liu, D.D. Mishra, X. Wang, H. Peng, C. Hu, Towards highly efficient solar-driven interfacial evaporation for desalination. J. Mater. Chem. A **8**(35), 17907 (2020)
13. H. Ghasemi, G. Ni, A.M. Marconnet, J. Loomis, S. Yerci, N. Miljkovic, G. Chen, Solar steam generation by heat localization. Nat. Commun. **5**(1), 1 (2014)
14. L. Zhou, Y. Tan, D. Ji, B. Zhu, P. Zhang, J. Xu, Q. Gan, Z. Yu, J. Zhu, Self-assembly of highly efficient, broadband plasmonic absorbers for solar steam generation. Sci. Adv. **2**(4), e1501227 (2016)
15. L. Zhou, Y. Tan, J. Wang, W. Xu, Y. Yuan, W. Cai, S. Zhu, J. Zhu, 3D self-assembly of aluminium nanoparticles for plasmon-enhanced solar desalination. Nat. Photonics **10**(6), 393 (2016)
16. K. Bae, G. Kang, S.K. Cho, W. Park, K. Kim, W.J. Padilla, Flexible thin-film black gold membranes with ultrabroadband plasmonic nanofocusing for efficient solar vapour generation. Nat. Commun. **6**(1), 1 (2015)
17. C. Chang, M. Liu, L. Pei, G. Chen, Z. Wang, Y. Ji, Porous TiNO solar-driven interfacial evaporator for high-efficiency seawater desalination. AIP Adv. **11**(4), 045228 (2021)
18. X. Hu, W. Xu, L. Zhou, Y. Tan, Y. Wang, S. Zhu, J. Zhu, Tailoring graphene oxide-based aerogels for efficient solar steam generation under one sun. Adv. Mater. **29**(5), 1604031 (2017)
19. F. He, M. Han, J. Zhang, Z. Wang, X. Wu, Y. Zhou, L. Jiang, S. Peng, Y. Li, A simple, mild and versatile method for preparation of photothermal woods toward highly efficient solar steam generation. Nano Energy **71**, 104650 (2020)
20. H. Ren, M. Tang, B. Guan, K. Wang, J. Yang, F. Wang, M. Wang, J. Shan, Z. Chen, D. Wei, Hierarchical graphene foam for efficient omnidirectional solar–thermal energy conversion. Adv. Mater. **29**(38), 1702590 (2017)
21. C. Chang, P. Tao, B. Fu, J. Xu, C. Song, J. Wu, W. Shang, T. Deng, Three-dimensional porous solar-driven interfacial evaporator for high-efficiency steam generation under low solar flux. ACS Omega **4**(2), 3546 (2019)
22. X. Li, W. Xu, M. Tang, L. Zhou, B. Zhu, S. Zhu, J. Zhu, Graphene oxide-based efficient and scalable solar desalination under one sun with a confined 2D water path. Proc. Natl. Acad. Sci. **113**(49), 13953 (2016)
23. T.A. Cooper, S.H. Zandavi, G.W. Ni, Y. Tsurimaki, Y. Huang, S.V. Boriskina, G. Chen, Contactless steam generation and superheating under one sun illumination. Nat. Commun. **9**(1), 1 (2018)

24. C. Chang, P. Tao, J. Xu, B. Fu, C. Song, J. Wu, W. Shang, T. Deng, High-efficiency superheated steam generation for portable sterilization under ambient pressure and low solar flux. ACS Appl. Mater. Interfaces **11**(20), 18466 (2019)
25. L. Zhu, M. Gao, C.K.N. Peh, X. Wang, G.W. Ho, Self-contained monolithic carbon sponges for solar-driven interfacial water evaporation distillation and electricity generation. Adv. Energy Mater. **8**(16), 1702149 (2018)
26. Y. Zhang, D. Zhao, F. Yu, C. Yang, J. Lou, Y. Liu, Y. Chen, Z. Wang, P. Tao, W. Shang, Floating rGO-based black membranes for solar driven sterilization. Nanoscale **9**(48), 19384 (2017)
27. Y. Kuang, C. Chen, S. He, E.M. Hitz, Y. Wang, W. Gan, R. Mi, L. Hu, A high-performance self-regenerating solar evaporator for continuous water desalination. Adv. Mater. **31**(23), 1900498 (2019)
28. J. Xu, Z. Wang, C. Chang, B. Fu, P. Tao, C. Song, W. Shang, T. Deng, Solar-driven interfacial desalination for simultaneous freshwater and salt generation. Desalination **484**, 114423 (2020)
29. Z. Wang, Q. Ye, X. Liang, J. Xu, C. Chang, C. Song, W. Shang, J. Wu, P. Tao, T. Deng, Paper-based membranes on silicone floaters for efficient and fast solar-driven interfacial evaporation under one sun. J. Mater. Chem. A **5**(31), 16359 (2017)
30. P. Yang, K. Liu, Q. Chen, J. Li, J. Duan, G. Xue, Z. Xu, W. Xie, J. Zhou, Solar-driven simultaneous steam production and electricity generation from salinity. Energy Environ. Sci. **10**(9), 1923 (2017)
31. L. Zhu, T. Ding, M. Gao, C.K.N. Peh, G.W. Ho, Shape conformal and thermal insulative organic solar absorber sponge for photothermal water evaporation and thermoelectric power generation. Adv. Energy Mater. **9**(22), 1900250 (2019)
32. X. Shan, A. Zhao, Y. Lin, Y. Hu, Y. Di, C. Liu, Z. Gan, Low-cost, scalable, and reusable photothermal layers for highly efficient solar steam generation and versatile energy conversion. Adv. Sustain. Syst. **4**(5), 1900153 (2020)
33. C. Chang, C. Yang, Y. Liu, P. Tao, C. Song, W. Shang, J. Wu, T. Deng, Efficient solar-thermal energy harvest driven by interfacial plasmonic heating-assisted evaporation. ACS Appl. Mater. Interfaces **8**(35), 23412 (2016)
34. F. Cao, K. McEnaney, G. Chen, Z. Ren, A review of cermet-based spectrally selective solar absorbers. Energy Environ. Sci. **7**(5), 1615 (2014)
35. P. Mu, Z. Zhang, W. Bai, J. He, H. Sun, Z. Zhu, W. Liang, A. Li, Superwetting monolithic hollow-carbon-nanotubes aerogels with hierarchically nanoporous structure for efficient solar steam generation. Adv. Energy Mater. **9**(1), 1802158 (2019)
36. Z. Yin, H. Wang, M. Jian, Y. Li, K. Xia, M. Zhang, C. Wang, Q. Wang, M. Ma, Q.-S. Zheng, Extremely black vertically aligned carbon nanotube arrays for solar steam generation. ACS Appl. Mater. Interfaces **9**(34), 28596 (2017)
37. F. Gong, W. Wang, H. Li, D.D. Xia, Q. Dai, X. Wu, M. Wang, J. Li, D.V. Papavassiliou, R. Xiao, Solid waste and graphite derived solar steam generator for highly-efficient and cost-effective water purification. Appl. Energy **261**, 114410 (2020)
38. Z. Wang, H. Liu, F. Chen, Q. Zhang, A three-dimensional printed biomimetic hierarchical graphene architecture for high-efficiency solar steam-generation. J. Mater. Chem. A **8**(37), 19387 (2020)
39. J. Chen, J.L. Yin, B. Li, Z. Ye, D. Liu, D. Ding, F. Qian, N.V. Myung, Q. Zhang, Y. Yin, Janus evaporators with self-recovering hydrophobicity for salt-rejecting interfacial solar desalination. ACS Nano **14**(12), 17419 (2020)
40. J. Zhao, Y. Yang, C. Yang, Y. Tian, Y. Han, J. Liu, X. Yin, W. Que, A hydrophobic surface enabled salt-blocking 2D Ti_3C_2 MXene membrane for efficient and stable solar desalination. J. Mater. Chem. A **6**(33), 16196 (2018)
41. G. Ni, S.H. Zandavi, S.M. Javid, S.V. Boriskina, T.A. Cooper, G. Chen, A salt-rejecting floating solar still for low-cost desalination. Energy Environ. Sci. **11**(6), 1510 (2018)
42. Q. Zhang, H. Yang, X. Xiao, H. Wang, L. Yan, Z. Shi, Y. Chen, W. Xu, X. Wang, A new self-desalting solar evaporation system based on a vertically oriented porous polyacrylonitrile foam. J. Mater. Chem. A. **7**(24), 14620 (2019)
43. L. Wilcox, *Guidelines for Drinking Water Quality, Recommendations* (WHO, Geneva, 1948)